Theoretical prediction of perfect spin filtering at interfaces between close-packed surfaces of Ni or Co and graphite or graphene

V. M. Karpan,[1] P. A. Khomyakov,[1] A. A. Starikov,[1] G. Giovannetti,[1,2] M. Zwierzycki,[3] M. Talanana,[1] G. Brocks,[1] J. van den Brink,[2,4] and P. J. Kelly[1]

[1]*Faculty of Science and Technology and MESA+ Institute for Nanotechnology, University of Twente, P.O. Box 217, 7500 AE Enschede, The Netherlands*

[2]*Instituut-Lorentz for Theoretical Physics, Universiteit Leiden, P.O. Box 9506, 2300 RA Leiden, The Netherlands*

[3]*Institute of Molecular Physics, P.A.N., Smoluchowskiego 17, 60-179 Poznań, Poland*

[4]*Institute for Molecules and Materials, Radboud Universiteit Nijmegen, P.O. Box 9010, 6500 GL Nijmegen, The Netherlands*

(Received 10 July 2008; published 19 November 2008)

The in-plane lattice constants of close-packed planes of fcc and hcp Ni and Co match that of graphite almost perfectly so that they share a common two-dimensional reciprocal space. Their electronic structures are such that they overlap in this reciprocal space for one spin direction only allowing us to predict perfect spin filtering for interfaces between graphite and (111) fcc or (0001) hcp Ni or Co. First-principles calculations of the scattering matrix show that the spin filtering is quite insensitive to amounts of interface roughness and disorder which drastically influence the spin-filtering properties of conventional magnetic tunnel junctions or interfaces between transition metals and semiconductors. When a single graphene sheet is adsorbed on these open *d*-shell transition-metal surfaces, its characteristic electronic structure, with topological singularities at the *K* points in the two-dimensional Brillouin zone, is destroyed by the chemical bonding. Because graphene bonds only weakly to Cu which has no states at the Fermi energy at the *K* point for either spin, the electronic structure of graphene can be restored by dusting Ni or Co with one or a few monolayers of Cu while still preserving the ideal spin-injection property.

DOI: 10.1103/PhysRevB.78.195419 PACS number(s): 73.43.Qt, 75.47.−m, 81.05.Uw, 72.25.−b

I. INTRODUCTION

We recently predicted a perfect spin filtering effect for ultrathin films of graphite sandwiched between two ferromagnetic leads.[1] This prediction emerged from two rapidly developing branches of condensed-matter physics: magnetoelectronics[2] and graphene electronics.[3] Magnetoelectronics exploits the additional degree of freedom presented by the intrinsic spin and associated magnetic moment of electrons while graphene electronics is based upon the unique electronic properties of two-dimensional graphene sheets. Based on the giant magnetoresistance (MR) effect discovered twenty years ago,[4,5] magnetoelectronics was rapidly applied to making improved read head sensors for hard disk recording and is a promising technology for a new type of magnetic storage device, a magnetic random access memory. The giant magnetoresistance (GMR) effect is based on the spin dependence of the transmission through interfaces between normal and ferromagnetic metals (FM). The effect is largest when the current passes through each interface in a so-called current-perpendicular-to-the-plane (CPP) measuring configuration but the absolute resistance of metallic junctions is too small for practical applications and the current-in-plane (CIP) configuration with a much smaller MR is what is used in practice. Replacing the nonmagnetic metal spacer with a semiconductor[6] or insulator (I), such as Al_2O_3 (Refs. 7 and 8) results in spin-dependent tunneling and much larger resistances are obtained with FM|I|FM magnetic tunnel junctions (MTJs). Substantial progress has been made in increasing the tunneling MR effect by replacing the amorphous Al_2O_3 insulator with crystalline MgO.[9,10] Though there is a relatively large lattice mismatch of 3.8% between Fe and MgO, the tunneling magnetoresistance (TMR) in Fe|MgO|Fe junctions has been reported to reach values as high as 180% at room temperature.[11] Low temperature values as high as 1010% have been reported for FeCoB|MgO|FeCoB MTJs.[12,13] The sensitivity of TMR (and spin injection) to details of interface structure[14,15] makes it difficult to close the quantitative gap between theory and experiment so it is important for our understanding of TMR to be able to prepare interfaces where disorder does not dominate the spin filtering properties. This remains a challenge due to the high reactivity of the open-shell transition-metal (TM) ferromagnets Fe, Co, and Ni with typical semiconductors and insulators.

With this in mind, we wish to draw attention to a quite different material system in which a thin graphite film is sandwiched between two ferromagnetic leads. Graphite is the ground state of carbon, and as one of the most important elemental materials, its electronic structure has been studied in considerable detail. It consists of weakly interacting sheets of carbon atoms strongly bonded in a very characteristic honeycomb structure. Because of the weak interaction between these "graphene" or "monolayer graphite" sheets, the electronic structure of graphite is usually discussed in two steps: first, in terms of the electronic structure of a single sp^2-bonded sheet, followed by consideration of the interaction between sheets.[16–18] From these early and many subsequent studies, it is known that graphene is a "zero-gap semiconductor" or a semimetal in which the Fermi surface is a point at the "*K*" point in the two-dimensional reciprocal space. The physical properties associated with this peculiar electronic structure have been studied theoretically in considerable detail, in particular in the context of carbon nanotubes

TABLE I. Lattice constants of Co, Ni, Cu, and graphite, $a_{\mathrm{hex}} \equiv a_{\mathrm{fcc}}/\sqrt{2}$. Equilibrium separation d_0 for a single graphene sheet on top of the graphite (0001) and Co, Ni, or Cu fcc (111) surfaces as calculated within the framework of the DFT-LDA using the in-plane lattice constant $a_{\mathrm{hex}}=2.46$ Å.

	Graphite	Co	Ni	Cu
$a_{\mathrm{fcc}}^{\mathrm{expt}}$ (Å)		3.544[a]	3.524[a]	3.615[a]
$a_{\mathrm{hex}}^{\mathrm{expt}}$ (Å)	2.46	2.506	2.492	2.556
$a_{\mathrm{hex}}^{\mathrm{LDA}}$ (Å)	2.45	2.42	2.42	2.49
d_0 (Å)	3.32	2.04	2.03	3.18

[a]Reference 28.

which can be considered as rolled-up graphene sheets.[19] With the very recent discovery and development of an exceptionally simple procedure for preparing single and multiple graphene sheets, micromechanical cleavage,[20] it has become possible to probe these predictions experimentally. Single sheets of graphene turn out to have a very high mobility[21] that manifests itself in a variety of spectacular transport phenomena such as a minimum conductivity, anomalous quantum Hall effect (QHE),[22,23] bipolar supercurrent,[24] and room-temperature QHE.[25] Spin injection into graphene using ferromagnetic electrodes has already been realized.[26,27] The weak spin-orbit interaction implied by the low atomic number of carbon should translate into very long intrinsic spin-flip scattering lengths, a very desirable property in the field of spin electronics or "spintronics," which aims to combine traditional semiconductor-based electronics with control over spin degrees of freedom. However, the room-temperature two-terminal MR effect of ~10% observed in lateral, current-in-plane graphene-based devices with soft permalloy leads is still rather small.[26]

Instead of a CIP geometry, we consider a CPP TM|Gr|TM (111) junction, where TM is a close-packed surface of fcc or hcp Ni or Co and Gr is graphite (or n sheets of graphene, Gr_n). We argue that such a junction should work as a perfect spin filter. The essence of the argument is given by Table I and Fig. 1. According to Table I, the surface lattice constants of (111) Ni, Co, and Cu match the in-plane lattice constants of graphene and graphite almost perfectly. The lattice mismatch of 1.3% at the Ni(111)|Gr interface is, in fact, one of the smallest for the magnetic junctions that have been studied so far. This small lattice mismatch suggests that epitaxial TM|Gr|TM junctions might be realized experimentally, for example using chemical vapor deposition.[29–31] Assuming perfect lattice matching at the TM|Gr interface, it is possible to directly compare the Fermi-surface projection of graphite with the projections of the Fermi surfaces (FS) of fcc Cu and of fcc and hcp Ni and Co onto close-packed planes, see Fig. 1.

The Fermi surface of graphene is a point at the high-symmetry K point in reciprocal space. The Fermi surfaces of graphite and of doped graphene are centered on this point and close to it. Figure 1 shows that there are no majority-spin states for Ni and Co close to the K point whereas minority-spin states exist (almost) everywhere in the surface Brillouin zone (BZ). Only the minority-spin channel should then contribute to transmission from a close-packed TM surface into graphite. In a TM|Gr|TM junction, electrons in other regions of reciprocal space on the left electrode would have to tunnel through graphite to reach the right electrode. If the graphite film is taken thick enough to suppress tunneling, majority-spin conductance will be quenched and only minority-spin conductance through the graphite will survive i.e., perfect spin filtering will occur when the magnetizations are aligned in parallel (P). For antiparallel (AP) alignment, the conductance will vanish.

In this paper, we wish to study the effectiveness of this spin filtering quantitatively; how it depends on the thickness of the graphite film, the geometry of the clean metal-graphite interface, interface roughness and disorder, and lattice mismatch. While we will be mainly concerned with the CPP geometry, we will also comment on the applicability of some

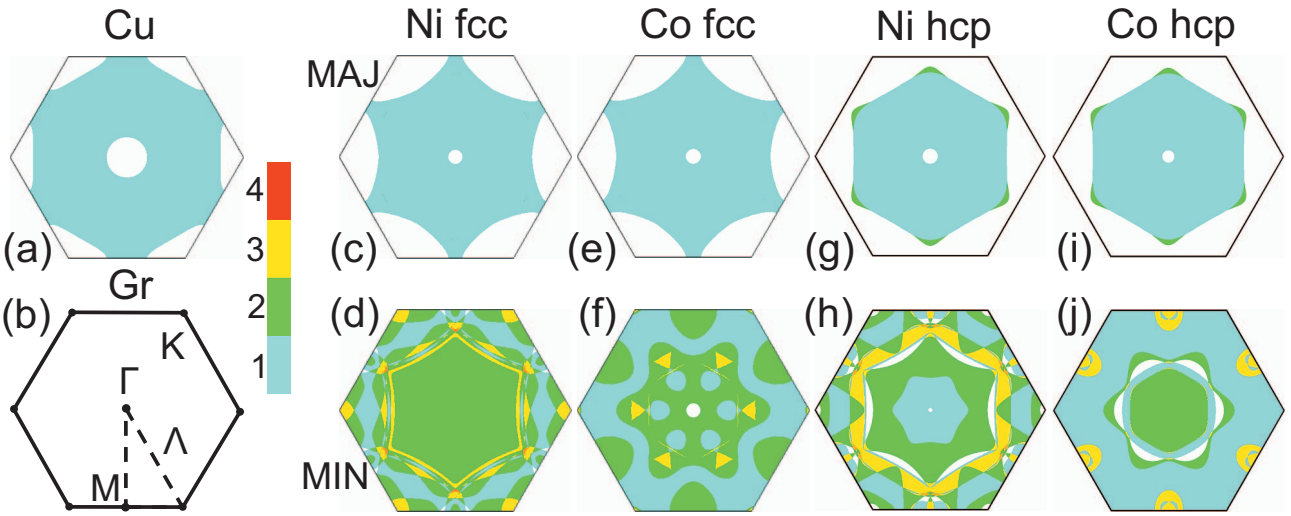

FIG. 1. (Color) Fermi-surface projections onto close-packed planes for: (a) fcc Cu; (c) majority- and (d) minority-spin fcc Ni (111); (e) majority- and (f) minority-spin fcc Co (111); (g) majority- and (h) minority-spin hcp Ni (0001); (i) majority- and (j) minority-spin hcp Co (0001). For graphene and graphite, surfaces of constant energy are centered on the K point of the two-dimensional interface Brillouin zone (b). The number of Fermi-surface sheets is given by the color bar.

of our conclusions to the CIP geometry. The paper is organized as follows. In Sec. II we give a brief description of the computational method and outline the most important technical details of the calculations. The transport formalism we use is based upon a very efficient minimal basis of tight-binding muffin-tin orbitals (TB-MTO) in combination with the atomic spheres approximation (ASA).[32] While the ASA works well for close-packed structures, some care is needed in using it for very open structures like that of graphite. In Sec. III we therefore benchmark the electronic structures calculated using the TB-LMTO-ASA method with those obtained from plane-wave pseudopotential (PWP) calculations. Section IV contains the results of spin-dependent electron-transport calculations for specular interfaces (ideal junction) as well as for junctions with interface roughness and alloy disorder. A summary is given and some conclusions are drawn in Sec. V.

II. COMPUTATIONAL METHOD

The starting point for our study is an atomic structure calculated by minimizing the total energy within the local spin density approximation (LSDA) of density-functional theory (DFT). This was done using a PWP method based upon projector augmented wave (PAW) pseudopotentials[33] as implemented in the VASP program.[34–36] The interaction between graphite and the TM surface is modeled using a repeated slab geometry of six metal layers with a graphene sheet on top and a vacuum thickness of ~ 12 Å. To avoid interactions between periodic images of the slab, a dipole correction is applied.[37] The surface Brillouin zone (SBZ) was sampled with a 36×36 **k**-point grid and the SBZ integrals carried out with the tetrahedron integration scheme.[38] A plane-wave kinetic-energy cutoff of 400 eV was used. The plane-wave pseudopotential calculations yield energy-band structures, charge transfers, binding energies, and work functions for single TM$|$Gr interfaces.[1,39] The equilibrium distances d_0 between the graphene sheet and the TM surfaces are summarized in Table I.

The equilibrium geometries are used as input for self-consistent TB linearized MTO (TB-LMTO) (Ref. 32) calculations for the TM$|$Gr$_n|$TM junction. The resulting Kohn-Sham potentials are used to calculate spin-dependent transmission probabilities through the TM$|$Gr$_n|$TM junction using a TB-MTO wave-function matching[40,41] scheme.[42–44] To do this, the junction is divided into three parts consisting of a scattering region sandwiched between semi-infinite left and right leads, all of which are divided into layers that are periodic in the lateral direction. The leads are assumed to be ideal periodic crystals in which the electron states (modes) are wave functions with Bloch translational symmetry. By making use of its Bloch symmetry, a semi-infinite lead can be represented as an energy-dependent non-Hermitian potential on the boundary of the scattering region so that the infinite system is made finite. According to the Landauer-Büttiker formalism of transport, the conductance can be calculated by summing up all the probabilities for transmitting an electron from the electron modes in the left lead through the junction into electron modes in the right leads.[43,45,46]

The effect of various types of disorder on the transmission can be studied using the same formalism and computer codes by modeling the disorder within large lateral supercells[42,43] and averaging over many configurations of disorder generated by choosing positions of impurity atoms or imperfections randomly. We study three types of disorder: interface roughness, interface alloying, and lattice mismatch. In the first two cases, averaging is performed over a minimum of ten configurations of disorder. To model interface roughness, some surface atoms are removed (replaced by "empty spheres" with nuclear charges that are zero in the ASA) and the ASA potentials are calculated self-consistently using a layer version[47] of the coherent-potential approximation (CPA).[48] The effect of interface alloying which might occur if deposition of a thin layer of Cu on Ni or Co ("dusting") leads to intermixing is modeled in a similar fashion. Third, the small lattice mismatch between graphite and TM is modeled by "cutting and pasting" AS potentials from self-consistent calculations for TM$|$Gr$_n|$TM junctions with two different in-plane lattice constants. The two systems are then combined using a supercell whose size is determined by the lattice mismatch. For self-consistent TB-LMTO-ASA calculations, the BZ of lateral supercells is sampled with a density roughly corresponding to a 24×24 **k**-point grid for a 1×1 interface unit cell. To converge the conductance, denser grids containing 800×800, 20×20, and 8×8 **k** points are used for 1×1 (ideal junction), 5×5 and 20×20 lateral supercells, respectively.

III. GEOMETRY AND ELECTRONIC STRUCTURE OF TM$|$Gr$_n|$TM

In this section we describe in more detail how the electronic structure of TM$|$Gr$_n|$TM junctions for TM=Cu, Ni, or Co is calculated. These close-packed metals can be grown with *ABC* stacking in the (111) direction (fcc), or with *AB* stacking in the (0001) direction (hcp). We neglect the small lattice mismatch of 1.3%, 1.9%, and 3.9% for the Ni$|$Gr, Co$|$Gr, and Cu$|$Gr interfaces, respectively, and assume the junction in-plane lattice constant to be equal to that of graphite, $a_{\mathrm{Gr}}=2.46$ Å. In the atomic spheres approximation, the atomic sphere radii of Ni, Co, and Cu are then $r_{\mathrm{TM}}=2.574$ a.u. The ASA works well for transition metals such as Co, Ni, or Cu which have close-packed structures. For materials such as graphite which has a very open structure with an in-plane lattice constant $a_{\mathrm{Gr}}=2.46$ Å, and an out-of-plane lattice constant $c_{\mathrm{Gr}}=6.7$ Å, the unmodified ASA is not sufficient. Fortunately, a reasonable description of the crystal potential can be obtained by packing the interstitial space with empty spheres.[49] This procedure should satisfy the following criteria: (i) the total volume of all atomic spheres has to be equal to the volume of the entire system (space filling), and the (ii) overlap between the atomic spheres should be as small as possible.

A. Graphite and graphene

To see how this procedure works in practice, we benchmark the TB-LMTO-ASA band structure of graphite against

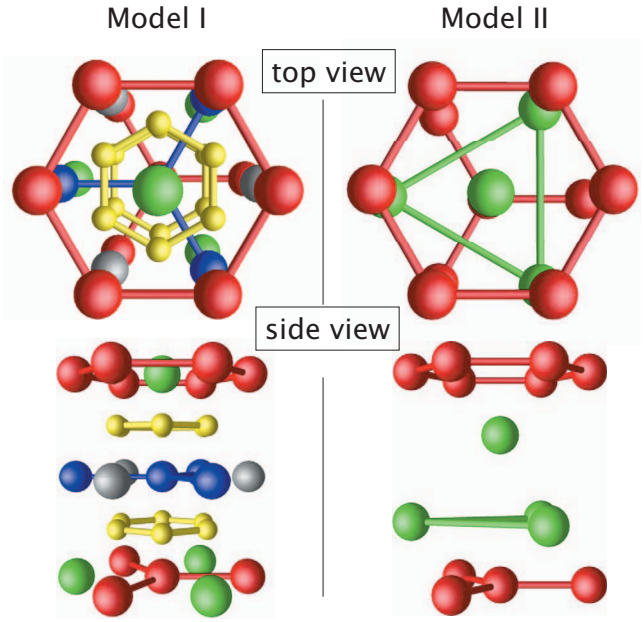

FIG. 2. (Color) Top and side perspective views (top and bottom panels) of graphite where the potential is represented in the atomic spheres approximation using additional, empty atomic spheres. Model I (left) contains 32 empty spheres in a unit cell containing four carbon atoms (red spheres). Model II (right), contains just four empty spheres. For model I, gray, green, blue, and yellow spheres display the positions of the empty spheres E_1, E_2, E_3 and E_4, respectively. For model II, there is just one type of empty sphere (green).

the "exact" band structure calculated with the PWP method. To preserve the graphite D_{6h}^4 $(P6_3/mmc)$ space-group symmetry,[50] the positions of the atomic spheres are chosen at Wyckoff positions. There are twelve different Wyckoff positions consistent with D_{6h}^4 symmetry and the best choice of empty spheres is not immediately obvious. We construct two models that describe the band structure close to the Fermi energy well compared to the PWP results; this is what is most relevant for studying transport in the linear-response regime. Model I with 32 empty spheres per unit cell and model II with only four empty spheres per unit cell both preserve the symmetry of graphite within the ASA. The crystal structures of graphite packed with empty spheres according to these two models is shown schematically in Fig. 2. Note that not all the empty spheres in a unit cell are shown in the figure. The Wyckoff labels, atomic sphere coordinates, and radii are given in Table II. Figure 3 shows the band structure of graphite obtained with the TB-LMTO-ASA for models I and II compared to the "exact" PWP band structure. Both models are seen to describe the graphite π bands around the Fermi energy very well. Model I provides a very good description of the bands within ± 2 eV of the Fermi energy, while the smaller basis model II is quite good within ± 1 eV. At the cost of including many more empty spheres, model I provides a better description of the crystal potential between the graphene planes than model II. For this reason we use model I to study the transport properties of ideal junctions, junctions with interface roughness and alloy disorder. To be able to handle the large 20×20 lateral supercells

TABLE II. Wyckoff symbols, standardized position parameters and atomic sphere radii for carbon atoms, C, and empty spheres, E (with nuclear charge Z=0), for two structural models of graphite with space group $D_{6h}^4(P6_3/mmc)$ (Ref. 50). Model I contains four different types of empty sphere: E_1, E_2, E_3, E_4; model II only one, E.

Model	Atom	Wyckoff position	Position parameters	Radius (a.u.)
I	C_1	$2b$		1.56
	C_2	$2c$		1.56
	E_1	$2a$		1.4
	E_2	$2d$		1.6
	E_3	$4f$	$z=0.5$	1.4
	E_4	$24l$	$x=1/3$, $y=0$, z=0.38	0.9
II	C_1	$2b$		1.56
	C_2	$2c$		1.56
	E	$4f$	$z=0.4$	2.18

needed to model a lattice mismatch of 5% at the TM|Gr interface, we use model II.

B. Graphene on Ni(111) substrate

The next step is to put a monolayer of graphite (graphene) on top of the Ni(111) substrate at a distance d_0 from the metal surface. From our studies of the energetics of graphene on TM(111), we found[1,39] that the lowest energy configuration (with $3m$ symmetry) for TM=Ni or Co corresponds to an "AC" configuration in which one carbon atom is positioned on top of a surface TM atom (an "A" site) while the second carbon atom is situated above a third layer TM atom (a "C" site), where A and C refer to the ABC stacking of fcc close-packed planes, see Fig. 4. This is in agreement with another recent first-principles calculation[51] as well as with experiments[30,31] for graphene on the Ni(111) surface. The electronic structure of a single graphene sheet will depend on d_0 and the details of such graphene-metallic substrate contacts can be expected to play an important role in current-in-plane devices.[26,27] For the less strongly bound BC configuration of Gr on Ni, the equilibrium separation is rather large, $d_0 \sim 3.3$ Å and the characteristic band structure of an isolated graphene sheet is clearly recognizable; see Fig. 5. For

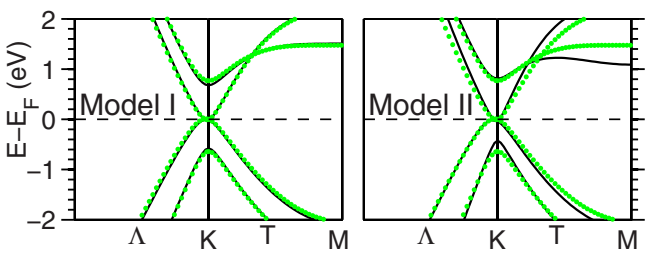

FIG. 3. (Color online) Band structure of graphite for model I on the left and model II on the right. (Green) dots and (black) lines correspond to band structures calculated using the PWP and TB-LMTO-ASA methods, respectively.

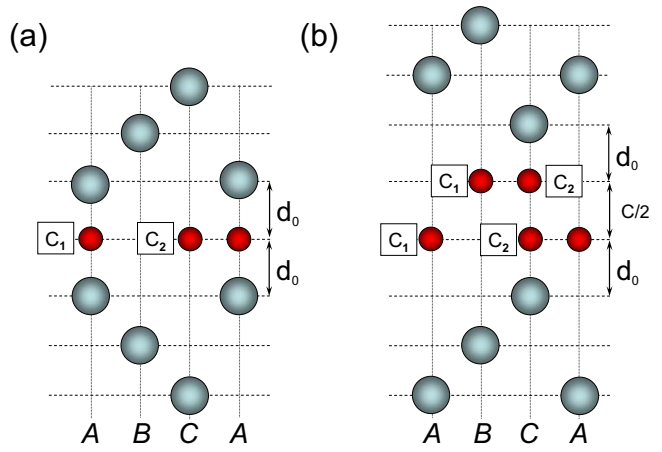

FIG. 4. (Color online) *AC* model of TM|Gr_n|TM structure for (a) odd and (b) even numbers of graphene sheets. Carbon atoms are represented by small dark (red) spheres, TM atoms by larger gray spheres. The configuration shown in (a) is a C_1C_1 configuration with the carbon atom labeled C_1 above an "*A*" site surface layer TM atom of the top and the bottom electrodes. The other carbon atom, C_2, is above a third layer TM atom on a "*C*" site. An equivalent C_2C_2 configuration in which the C_2 atoms are on top of "*A*" site TM atoms can be realized by rotating the top and bottom electrodes by 180° about a vertical axis through the second layer "*B*" sites; this effectively interchanges C_1 and C_2. Two other equivalent configurations C_1C_2 and C_2C_1 can be realized in an analogous fashion by rotating either the top or the bottom electrode through 180°. For two sheets of graphene stacked as in graphite, a C_2C_2 configuration is sketched in (b). Interlayer distance is indicated as d_0 and $c/2$ is the distance separating two neighboring graphene sheets.

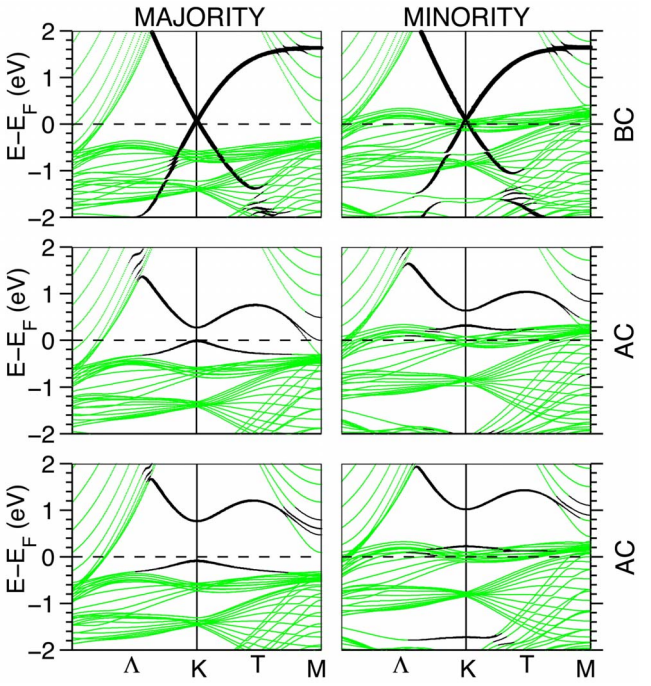

FIG. 5. (Color online) The results of PWP (top and middle rows) and TB-LMTO-ASA (bottom row) calculations of majority- (left panels) and minority- (right panels) spin band structures (green) of single graphene layers absorbed on both sides of a 13 layer (111) Ni slab for a *BC* configuration with d_0=3.3 Å, (top) and an *AC* configuration with d_0=2.0 Å (middle and bottom). The bands are replotted and superimposed in black using the carbon p_z character as a weighting factor. The Fermi energy is indicated by the horizontal dashed line.

the lowest energy *AC* configuration, the interaction between the graphene sheet and Ni surface is much stronger, a gap is opened in the graphene derived p_z bands and at the Fermi energy there are no graphene states at the *K* point in reciprocal space for the minority-spin channel. This may complicate efficient spin injection into graphene in lateral, CIP devices.[26]

The band structure calculated with the TB-LMTO-AS approximation for the *AC* configuration is shown in the bottom panel of Fig. 5 and is seen to describe graphene on Ni(111) qualitatively quite well. However, the splitting of the graphene bands, which arises because the two carbons atoms are no longer equivalent when one is above a top layer *A* site Ni atom and the other is above a third layer *C* site Ni atom, is somewhat larger than that resulting from the PWP calculation.

C. Ni|Gr_n|Ni(111) junction

The transmission of electrons through a TM|Gr_n|TM junction will obviously depend on the geometry of the metal-graphite contacts. Rather than carrying out a total-energy minimization explicitly for every different value of *n*, we assume that the weak interaction between graphene sheets will not influence the stronger TM|Gr interaction and construct the junction using the *AC* configuration and the equilibrium separation d_0=2.03 Å for each interface, as shown in Fig. 4. The interstitial space at the TM|Gr interfaces is filled with empty spheres using a procedure analogous to that described for bulk graphite.[52]

Because the two carbon atoms C_1 and C_2 in the graphene unit cell are equivalent, either of them can be positioned above a surface Ni atom on an *A* site with the other on the *C* site in an "*AC*" configuration, without changing the total energy. Since this can be done for each TM|Gr interface separately, four different configurations of the TM|Gr|TM junction can be constructed by rotating one or both electrodes through 180° about a vertical axis through the second layer *B* sites which interchanges electrode *A* and *C* sites in Fig. 4. We label these four different configurations C_1C_1, C_1C_2, C_2C_1, and C_2C_2 in terms of the carbon atoms which are bonded to *A* site TM atoms. For more than one graphene sheet, the second sheet breaks the symmetry between the C_1 and C_2 atoms. While we have not checked this explicitly, we expect the corresponding energy difference to be small and neglect it.

In Fig. 5 we saw that the graphene π states interacted strongly with the nickel surface in the minimum-energy *AC* configuration. The interaction with the metal substrate made the C_1 and C_2 carbon atoms inequivalent and led to the opening of an energy gap in the graphene π bands. Having constructed an interface geometry, we study the band structure of the Ni|graphene|Ni (111) junction as a function of $\mathbf{k}_\parallel$, the two-dimensional Bloch vector, modeling it as a Ni_3|graphene|Ni_3 junction repeated periodically in the (111)

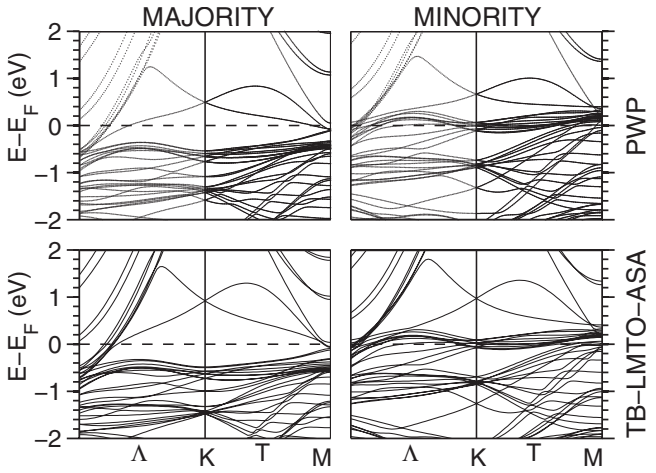

FIG. 6. Energy band structures of an ideal $Ni_6|Gr$ (111) multilayer with six layers of fcc Ni sandwiching a single graphene sheet in a C_1C_2 configuration, for majority (left panels) and minority (right panels) spin channels. Plane wave pseudopotential calculations are shown on top (dotted lines), the TB-LMTO-ASA results on the bottom (solid lines).

direction (which is equivalent to a $Ni_6|Gr_1$ multilayer). The bands in the top panels of Fig. 6 were calculated using the benchmark PWP method, those in the bottom panels with the TB-LMTO-ASA. We see that the Ni-related bands are described well by the TB-LMTO-ASA as might be expected since the ASA is known to work well for close-packed solids. The second thing we see is that there is no gap in the graphene π bands. This is because the C_1C_2 configuration used in the calculation has inversion symmetry and the equivalence between the two carbon atoms is restored; see Fig. 4(a). The third point to be made is that the charge transfer from graphene (work function: 4.5 eV) to Ni (work function: 5.5 eV) and strong chemisorption leads to the formation of a potential step at the interface and a significant shift of the graphene π bands with respect to the Fermi level[39] which is pinned at that of bulk Ni. We find similar results for $Co|Gr|Co(111)$ and $Co|Gr|Co(0001)$ junctions. There is a difference between the position of the graphene π-derived bands, most noticeably at the K point, in the PWP and TB-LMTO-ASA band structures shown in Fig. 6 for both spin channels. It appears that the interface dipole is not accurately described by the ASA. From the point of view of describing transmission of electrons through this junction, the electronic band structure is the most important measure of the quality of our basis, description of the potential, etc., so this discrepancy will most certainly have quantitative implications. Fortunately, our most important conclusions will be qualitative and will not depend on this aspect of the electronic structure.

IV. ELECTRON TRANSPORT THROUGH A FM|Gr_n|FM JUNCTION

Using the geometries and potentials described above, we proceed to study the spin-dependent transmission through ideal $Ni|Gr|Ni$ junctions in the CPP geometry as a function of the thickness of the graphite spacer layer. We then discuss

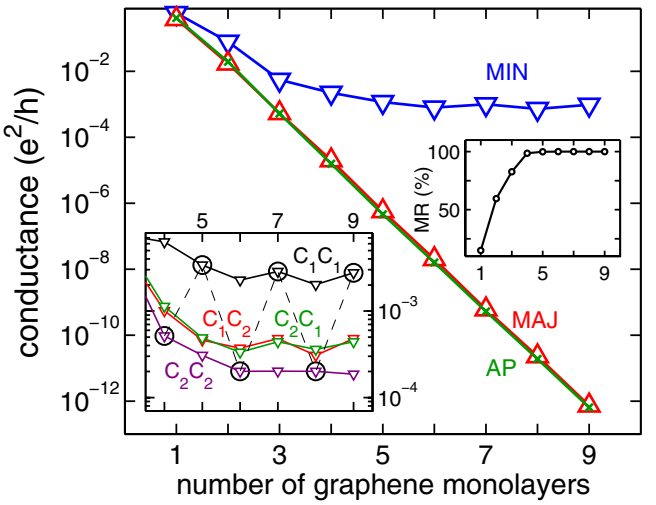

FIG. 7. (Color online) Conductances G_P^{min} (▽),G_P^{maj} (△), and G_{AP}^{σ} (×) averaged over the four configurations C_1C_1, C_1C_2, C_2C_1, and C_2C_2 of a $Ni|Gr_n|Ni$ junction as a function of the number of graphene monolayers n for ideal junctions. Right inset: magnetoresistance as a function of n. Left inset: minority parallel conductance G_P^{min} (▽) given for four different configurations. The points which are circled and connected with a dashed line are the values which were shown in Ref. 1.

how interface roughness, alloy disorder, and the lattice mismatch between graphite and the substrate affect the spin-filtering properties of the junctions using large lateral supercells to model the various types of disorder. Because very similar results are found for all the TMs shown in Fig. 1, we focus on fcc Ni as a substrate because it has the smallest lattice mismatch with graphite, and graphene has been successfully grown on Ni using chemical vapor deposition.[29,30]

A. Specular interface

The spin-dependent transmission through $Ni|Gr_n|Ni$ (111) junctions is shown in Fig. 7 for parallel and antiparallel orientations of the magnetization in the nickel leads, in the form of the conductances G_P^{σ} and G_{AP}^{σ} with σ=min, maj. All the conductance values are averaged over the four interface configurations of the $Ni|Gr_n|Ni$ junction which are consistent with AC configurations of the $Ni|Gr$ (111) interface. G_P^{maj} and G_{AP}^{σ} are strongly attenuated, while G_P^{min} saturates to an n-independent value. The magnetoresistance defined as

$$\mathrm{MR} = \frac{R_{AP} - R_P}{R_{AP}} \times 100\% \equiv \frac{G_P - G_{AP}}{G_P} \times 100\%, \qquad (1)$$

rapidly approaches its maximum possible value of 100%, as shown in the right inset in Fig. 7. This *pessimistic* definition of MR is more convenient here because G_{AP} vanishes for large n. It is usually the optimistic version, that approaches 10^{12}% in our calculations but does not saturate, that is quoted.[9,10,53,54] The left inset in Fig. 7 shows how the conductance depends on the particular configuration of the junction. The minority-spin conductance in the parallel configuration, which dominates the magnetoresistance behavior, is highest for the C_1C_1 configuration with an asymptotic value

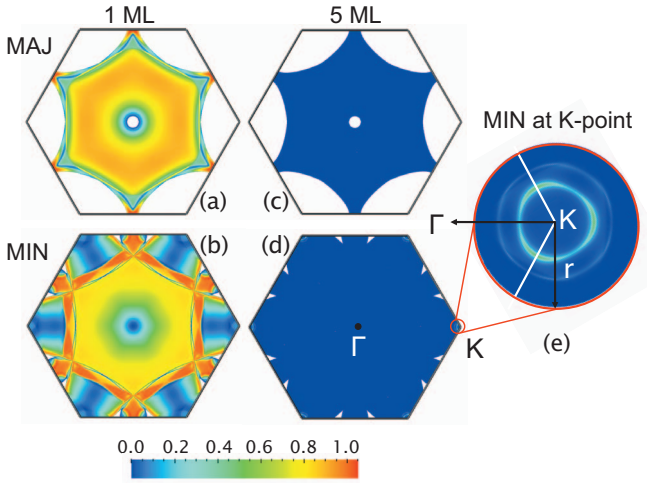

FIG. 8. (Color) Transmission as a function of the transverse crystal momentum $\mathbf{k}_\parallel$ in the two-dimensional interface BZ for a C_1C_2 configuration of an ideal Ni|Gr_n|Ni (111) junction in a parallel state. (a) and (b) are for a single graphene sheet, $n=1$; (c) and (d) are for $n=5$; (e) shows the minority-spin transmission in a small circle of radius $r=0.057(2\pi/a_{\mathrm{Gr}})$ around the K point for five ML of graphite on an enlarged scale.

of $G_{\mathrm{P}}^{\mathrm{min}} \sim 10^{-2} G_0$, where G_0 is the conductance unit equal to e^2/h. This is approximately an order of magnitude larger than $G_{\mathrm{P}}^{\mathrm{min}}$ for the C_2C_1, C_1C_2, and C_2C_2 configurations. The C_1C_2 and C_2C_1 configurations are equivalent so the corresponding values of $G_{\mathrm{P}}^{\mathrm{min}}$ should be identical. The small differences between these two configurations which can be seen in the figure are an indication of the overall accuracy of the numerical calculation. The points which are circled and connected with a dashed line are the oscillating values which were shown in Ref. 1.

To demonstrate that spin filtering occurs due to high transmission of minority-spin electrons around the K point, we plot the majority- and minority-spin transmission for the P configuration as a function of $\mathbf{k}_\parallel$ for two graphite films of different thickness in Fig. 8. A single sheet of graphene (a monolayer of graphite) is essentially transparent with a conductance of order G_0 in both spin channels. In the minority-spin channel, the transmission is very low or vanishes close to $\bar{\Gamma}$ and close to K along the high-symmetry Γ-K line, in spite of there being one or more sheets of Fermi surface in these regions of reciprocal space. This is a clear indication of the importance of matrix element effects: selection rules resulting from the incompatibility of wave functions on either side of the interface.[43]

The majority transmission must be zero around $\bar{\Gamma}$ and around the K point because there are no states there in the Ni leads. For thicker graphite, the only contribution to the majority-spin conductance comes from tunneling through graphite in regions of the two-dimensional Brillouin zone (2D-BZ) where there are Ni states and the gap between graphite bonding and antibonding π states is small. This occurs close to the M point;[55] see Fig. 3. Because the gap decreases going from M to K, the transmission increases in this direction. At the edge of the Fermi-surface projection, the velocity of the Bloch electrons in the leads is zero so that the maximum transmission occurs just on the M side of these edges (not shown).

The total minority transmission consists of two contributions. On the one hand there is a tunneling contribution from throughout the 2D-BZ which, depending on the particular $\mathbf{k}_\parallel$ point, is determined by the gap in graphite as well as by the compatibility of the symmetries, at that point, of the wave functions in Ni and in graphite. On the other hand there is a large transmission from the neighborhood of the K point coming from the Bloch states there in graphite. Once these have coupled to available states in Ni, this contribution does not change much as more layers of graphite are added. Perfect spin filtering (100% magnetoresistance) occurs when the tunneling contributions are essentially quenched compared to the minority-spin K point contribution. For four monolayers (MLs) of graphite the polarization is within a percent of 100% and for five MLs it is for all intents and purposes complete. The only discernible transmission in Figs. 8(c)–8(e) is found close to the K point. Magnification of this region in Fig. 8(e) shows a certain amount of structure in the transmission. This can be explained in terms of the multiple sheets of Ni minority-spin Fermi surface in the vicinity of K (Fig. 1) and the small but finite dispersion of the graphite bands perpendicular to the basal plane.[55] The transmission is seen to have the threefold symmetry of the junction.

The spin filtering does not depend on details of how graphite is bonded to the ferromagnetic leads as long as the translational symmetry parallel to the metal-graphite interfaces is preserved. We have verified this by performing explicit calculations (results not shown here) for junctions in the "*AB*" and "*BC*" configurations with different metal-graphite separations d.

B. Ni|Cu_m|Gr_n|Cu_m|Ni(111)

In Sec. III, we saw that the electronic structure of a sheet of graphene depends strongly on its separation from the underlying TM substrate. For Co and Ni, equilibrium separations of the order of 2.0 Å were calculated for the lowest energy AC configuration (see Table I), the interaction was strong and the characteristic linear dispersion of the graphene electronic structure was destroyed, Fig. 5. For a separation of 3.3 Å, the small residual interaction does not destroy the linear dispersion. Unlike Co and Ni, Cu interacts only weakly with graphene, there is only a small energy difference between the "asymmetric" AC configuration with $d_0=3.3$ Å and the slightly more weakly bound "symmetric" BC configuration with $d_0=3.4$ Å, and bonding to Cu preserves the characteristic graphene electronic structure, opening up only a very small gap of about 10 meV at the Dirac point.[56]

Should it be desirable to avoid forming a strong bond between graphite and the TM electrode, then it should be a simple matter of depositing one or a few layers of Cu on, e.g., Ni. Such a thin layer of Cu will adopt the in-plane lattice constant of Ni and graphite will bind to it weakly so that the electronic structure of the first layer of graphite will be only weakly perturbed. Because Cu oxidizes less readily than Ni or Co, it may be used as a protective layer. Cu has no

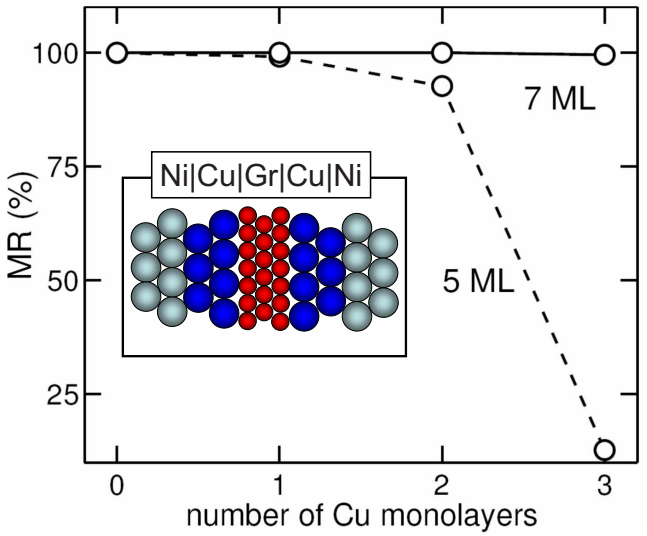

FIG. 9. (Color online) Magnetoresistance as a function of the number of Cu monolayers on both left and right Ni leads in case of five ML (dashed line) and seven ML (solid line) of graphene.

states at or around the K point for either spin channel (Fig. 1) so it will simply attenuate the conductance of the minority-spin channel at the K point. This is demonstrated in Fig. 9 where the magnetoresistance of a $\mathrm{Ni}|\mathrm{Cu}_m|\mathrm{Gr}_n|\mathrm{Cu}_m|\mathrm{Ni}$ junction is shown as a function of the number m of layers of Cu when there are five and seven MLs of graphite. As the thickness of Cu is increased, reducing the transmission of the minority-spin K point channel, the MR decreases. The reduction in the MR can be compensated by increasing the thickness of graphite. These conclusions are consistent with the qualitative conclusions drawn above in connection with Fig. 1(a).

Although the linear dispersion of the graphene bands is essentially unchanged by adsorption on Cu, application of an in-plane bias will destroy the translational symmetry parallel to the interface upon which our considerations have been based. The finite lateral size of a Ni|Cu electrode will also break the translational symmetry in a CIP measuring configuration and edge effects may destroy the spin-injection properties.

C. Effect of disorder

1. Lattice mismatch

So far, we have assumed TM and graphite lattices which are commensurate in plane. In practice there is a lattice mismatch with graphite of 1.3% for Ni, 1.9% for Co, and 3.9% for Cu which immediately poses the question of how this will affect the perfect spin filtering. While lattice mismatch between lattices with lattice constants a_1 and a_2 can in principle be treated by using n_1 units of lattice 1 and n_2 units of lattice 2 with $n_1a_1=n_2a_2$, in practice we cannot perform calculations for systems with n much larger than 20 which limits us to treating a large lattice mismatch of 5%. To put an upper limit on the effect of a 1.3%–1.9% lattice mismatch, we performed calculations for a $\mathrm{Ni}|\mathrm{Gr}_5|\mathrm{Ni}$ junction matching 19×19 unit cells of Ni in-plane to 20×20 unit cells of graphite. The effect of this 5% lattice mismatch was to reduce the (pessimistic) magnetoresistance from 100% to 90% (or ~900% in the optimistic definition). We conclude that the actual Ni|Gr mismatch of 1.3% should not be a serious limiting factor in practice.

2. Interface roughness

Incommensurability is not the only factor that might reduce the magnetoresistance. Preparing atomically perfect interfaces is not possible and raises the question of how sensitive the perfect spin filtering will be to interface roughness or disorder. Our studies of spin injection in Ref. 15 and TMR in Ref. 14 suggest they may be very important and can even dominate the spin transport properties.

The simplest way to prepare a CPP Ni|Gr|Ni junction would presumably be to begin with a (111) oriented Ni or Co crystal characterized on an atomic scale by scanning tunneling microscopy (STM) and atomic force microscopy (AFM), grow the required number of layers of graphene by, e.g., chemical vapor deposition,[29–31] and after characterization of the graphene layers to then deposit the second Ni electrode. To prepare a CIP junction, we envisage a procedure in which thin graphite layers are prepared by micromechanical cleavage of bulk graphite onto a SiO_2 covered Si wafer[57] into which TM (Ni or Co) electrodes have been embedded. We assume that the (111) electrodes can be prepared in ultrahigh vacuum and characterized on an atomic scale and that the surfaces are flat and defect free. Layers of graphene are peeled away until the desired value of n is reached.

Assuming it will be possible to realize one essentially perfect interface, we have studied the effect of roughness at the second interface, assuming it is prepared by evaporation or some similar method. The graphite is assumed to be atomically perfect and all of the roughness occurs in the metal interface layer. We model this roughness as in Ref. 14 by removing a certain percentage of the top layer atoms. The atomic sphere potentials are calculated using the layer version[47] of the coherent-potential approximation (CPA).[48] The CPA AS potentials are then distributed at random with the appropriate concentration in 5×5 lateral supercells and the transmission is calculated in a CPP geometry for a number of such randomly generated configurations. The effect on the magnetoresistance of removing half a monolayer of Ni is shown in Fig. 10 as a function of the number of graphite layers. 50% roughness at one interface is seen to reduce the 100% magnetoresistance to about 70% (~230% optimistic).

3. Interface disorder

The last type of disorder we consider is a layer of interface alloy. We imagine that depositing a layer of Cu on Ni to prevent graphite bonding to the Ni has led to a layer of Ni and Cu mixing. In a worst case scenario, we assume all of the disorder is in the surface layer and assume this to be a $Ni_{50}Cu_{50}$ random alloy. The potentials are once again calculated self-consistently using the layer CPA and the transmission calculated as for roughness. The effect on a monolayer of CuNi alloy is to reduce the MR to 90% (900% in the

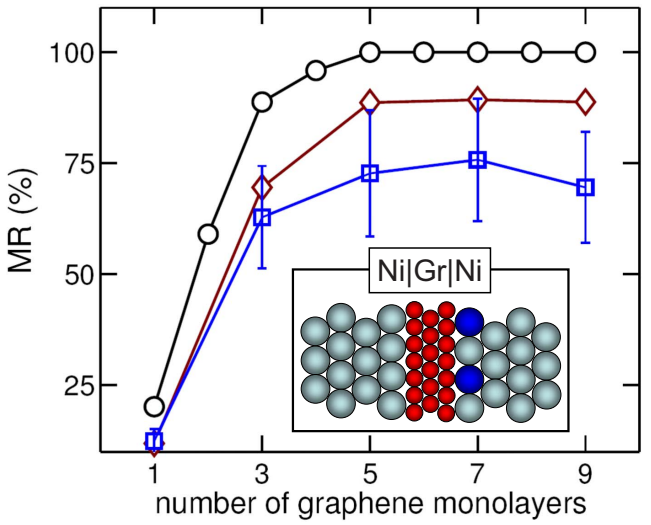

FIG. 10. (Color online) Magnetoresistance as a function of n for: ideal junctions (circles); Ni$|$Gr$_n|$Cu$_{50}$Ni$_{50}|$Ni junctions where the surface layer is a disordered alloy (diamonds); Ni$|$Gr$_n|$Ni junctions where the top layer of one of the electrodes is rough with only half of the top layer sites occupied (squares). For the rough surface layer, the error bars indicate the spread of MR obtained for different configurations. Inset: schematic representation of Ni$|$Gr$_n|$Ni junction with alloy disorder (roughness) at the right Ni$|$Gr interface. Ni atoms are given by large gray spheres while Cu (missing) atoms in the case of alloy disorder (roughness) are given by large dark (blue) spheres. Positions of carbon atoms are represented by small dark (red) spheres.

optimistic definition) for a thick graphite film, as shown in Fig. 10. These results indicate that the momentum transfer induced by the scattering due to imperfections is insufficient to bridge the large gap about the K point in the majority-spin FS projections.

Ideally, we should avoid interface roughness and disorder altogether. Since metal surfaces can be prepared with very little disorder, what is required is to be able to perform micromechanical cleavage on a metal surface rather than on SiO_2. If this were possible, two essentially perfect TM$|$Gr interfaces could perhaps be joined using a method analogous to vacuum bonding.[58] Alternatively, since graphite has a large c-axis resistivity[59] it may only be necessary to prepare one near-perfect Ni$|$graphite interface. If the graphite layer is sufficiently thick, then it should be possible to achieve 100% spin accumulation in a high-resistivity material making it suitable for injecting spins into semiconductors.[60] Because carbon is so light, spin-flip scattering arising from spin-orbit interaction should be negligible.

V. DISCUSSION AND CONCLUSIONS

Motivated by the recent progress in preparing and manipulating discrete, essentially atomically perfect graphene layers, we have used parameter-free, materials-specific electronic structure calculations to explore the spin transport properties of a novel TM$|$graphite system. Perfect spin filtering is predicted for ideal TM$|$Gr$_n|$TM junctions with TM=Co or Ni in both fcc and hcp crystal structures. The spin filtering stems from a combination of almost perfect matching of Gr and TM lattice constants and unique features of their electronic band structures. Graphite films have occupied states at the Fermi level only around the K point in the first (interface) BZ. Close-packed fcc and hcp Ni and Co have only minority-spin states in the vicinity of the same K point at the Fermi energy. For a modest number of layers of graphite, transport from one TM electrode to the other can only occur via the graphite states close to the K point and perfect spin filtering occurs if the in-plane translational symmetry is preserved. For majority spins, the graphite film acts as a tunnel barrier while it is conducting for minority-spin electrons, albeit with a small conductance.

Compared to a conventional magnetic tunnel junction, a TM$|$Gr$_n|$TM CPP junction has several important advantages. First, the lateral lattice mismatch is three times smaller than the 3.8% found for the now very popular Fe$|$MgO$|$Fe(001) MTJs.[13] This will reduce the number of defects caused by strain that otherwise limits the thickness of the tunnel barrier and degrades the efficiency of spin injection. Second, the spin polarization approaches 100% for an ideal junction with $n>3$ graphene layers, and is only reduced to 70%–90% for junctions with large interface roughness or disorder. Third, the spin-filtering effect should not be very sensitive to temperature. From Fig. 8(a) and the corresponding figures for other thicknesses of graphite, we see that the largest contribution to the majority-spin conduction comes from tunneling at the M point where bulk Co and Ni have propagating states at the Fermi level and the distance in energy to states in graphite with the same $\mathbf{k}_\parallel$ vector is a minimum. From Fig. 3 we see that the energy gap is almost 1 eV between the Fermi level and the closest graphite band at this point. To bridge the horizontal gap between states close to the K point in graphite and the closest states in Co or Ni requires an in-plane momentum transfer of order $\Delta k \sim \pi/a$. The corresponding energy would be (comparable to) that of an optical phonon which is large because of the stiffness of a graphene sheet.

To achieve perfect spin injection into a single sheet of graphene is more troublesome.[26,27] The electronic structure calculations presented here show that the carbon π orbitals hybridize strongly with Ni (and also Co) surfaces leading to the destruction of graphene's characteristic electronic structure. We have already suggested that dusting Ni (or Co) with Cu will lead to near-complete restoration of the graphene electronic structure because of the weak interaction between graphene and Cu. Moreover Cu might also prevent rapid oxidation of the Ni(Co) (111) surfaces, which could be important for making practical devices. However, application of a bias would lead to a breaking of the translational symmetry responsible for the perfect spin filtering. The finite size of electrodes might also present a problem in practice especially if the potential drop occurs at the edges. The problem can be simply solved by forcing the electric field to be perpendicular to the TM$|$graphite interface as sketched in Fig. 11 where the right electrode could equally well be placed on top of the graphite.

In conclusion, we propose a new class of lattice-matched junctions, TM$|$Gr$_n|$TM, that exhibit exceptionally high magnetoresistance effect which is robust with respect to interface

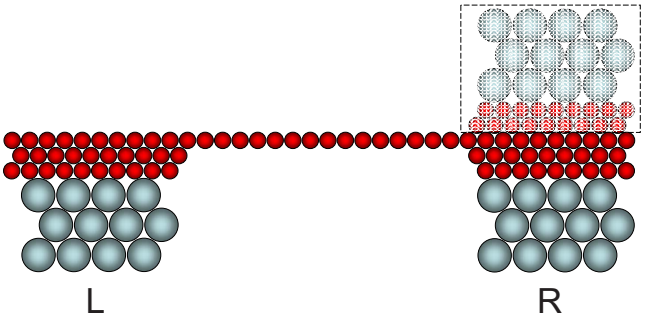

FIG. 11. (Color online) Schematic figure of a TM|Gr|TM CIP junction in which the electric field is forced to be essentially perpendicular to the TM|graphene interface. The dashed shaded box indicates an alternative configuration with the right-hand electrode on top of the graphene.

disorder, roughness, and finite temperatures making them highly attractive for possible applications in spintronic devices.

ACKNOWLEDGMENTS

This work is supported by "NanoNed," a nanotechnology program of the Dutch Ministry of Economic Affairs. It is part of the research programs of "Chemische Wetenschappen" (CW) and "Stichting voor Fundamenteel Onderzoek der Materie" (FOM) and the use of supercomputer facilities was sponsored by the "Stichting Nationale Computer Faciliteiten" (NCF), all financially supported by the "Nederlandse Organisatie voor Wetenschappelijk Onderzoek" (NWO). M.Z. wishes to acknowledge support from EU grant CARDEQ under Contract No. IST-021285-2.

[1] V. M. Karpan, G. Giovannetti, P. A. Khomyakov, M. Talanana, A. A. Starikov, M. Zwierzycki, J. van den Brink, G. Brocks, and P. J. Kelly, Phys. Rev. Lett. **99**, 176602 (2007).
[2] I. Žutić, J. Fabian, and S. D. Sarma, Rev. Mod. Phys. **76**, 323 (2004).
[3] A. H. C. Neto, F. Guinea, N. M. R. Peres, K. S. Novoselov, and A. K. Geim, arXiv:0709.1163, Rev. Mod. Phys. (to be published).
[4] M. N. Baibich, J. M. Broto, A. Fert, F. Nguyen Van Dau, F. Petroff, P. Etienne, G. Creuzet, A. Friederich, and J. Chazelas, Phys. Rev. Lett. **61**, 2472 (1988).
[5] G. Binasch, P. Grünberg, F. Saurenbach, and W. Zinn, Phys. Rev. B **39**, 4828 (1989).
[6] M. Julliere, Phys. Lett. **54A**, 225 (1975).
[7] J. S. Moodera, L. R. Kinder, T. M. Wong, and R. Meservey, Phys. Rev. Lett. **74**, 3273 (1995).
[8] T. Miyazaki and N. Tezuka, J. Magn. Magn. Mater. **139**, L231 (1995).
[9] S. Yuasa, T. Nagahama, A. Fukushima, Y. Suzuki, and K. Ando, Nature Mater. **3**, 868 (2004).
[10] S. S. P. Parkin, C. Kaiser, A. Panchula, P. M. Rice, B. Hughes, M. Samant, and S. H. Yang, Nature Mater. **3**, 862 (2004).
[11] S. Yuasa, T. Katayama, T. Nagahama, A. Fukushima, H. Kubota, Y. Suzuki, and K. Ando, Appl. Phys. Lett. **87**, 222508 (2005).
[12] Y. M. Lee, J. Hayakawa, S. Ikeda, F. Matsukura, and H. Ohno, Appl. Phys. Lett. **90**, 212507 (2007).
[13] S. Yuasa and D. D. Djayaprawira, J. Phys. D **40**, R337 (2007).
[14] P. X. Xu, V. M. Karpan, K. Xia, M. Zwierzycki, I. Marushchenko, and P. J. Kelly, Phys. Rev. B **73**, 180402(R) (2006).
[15] M. Zwierzycki, K. Xia, P. J. Kelly, G. E. W. Bauer, and I. Turek, Phys. Rev. B **67**, 092401 (2003).
[16] P. R. Wallace, Phys. Rev. **71**, 622 (1947).
[17] J. C. Slonczewski and P. R. Weiss, Phys. Rev. **109**, 272 (1958).
[18] W. M. Lomer, Proc. R. Soc. London, Ser. A **227**, 330 (1955).
[19] T. Ando, J. Phys. Soc. Jpn. **74**, 777 (2005).
[20] K. S. Novoselov, D. Jiang, F. Schedin, T. J. Booth, V. V. Khotkevich, S. V. Morozov, and A. K. Geim, Proc. Natl. Acad. Sci. U.S.A. **102**, 10451 (2005).
[21] K. S. Novoselov, A. K. Geim, S. V. Morozov, D. Jiang, Y. Zhang, S. V. Dubonos, I. V. Grigorieva, and A. A. Firsov, Science **306**, 666 (2004).
[22] K. S. Novoselov, A. K. Geim, S. V. Morozov, D. Jiang, M. I. Katsnelson, I. V. Grigorieva, S. V. Dubonos, and A. A. Firsov, Nature (London) **438**, 197 (2005).
[23] Y. B. Zhang, Y. W. Tan, H. L. Stormer, and P. Kim, Nature (London) **438**, 201 (2005).
[24] H. B. Heersche, P. Jarillo-Herrero, J. B. Oostinga, L. M. K. Vandersypen, and A. F. Morpurgo, Nature (London) **446**, 56 (2007).
[25] K. S. Novoselov, Z. Jiang, Y. Zhang, S. V. Morozov, H. L. Stormer, U. Zeitler, J. C. Maan, G. S. Boebinger, P. Kim, and A. K. Geim, Science **315**, 1379 (2007).
[26] E. W. Hill, A. K. Geim, K. Novoselov, F. Schedin, and P. Blake, IEEE Trans. Magn. **42**, 2694 (2006).
[27] N. Tombros, C. Jozsa, M. Popinciuc, H. T. Jonkman, and B. J. van Wees, Nature (London) **448**, 571 (2007).
[28] H. Ibach and H. Lüth, *Solid-State Physics*, 2nd ed. (Springer-Verlag, Berlin, 1995).
[29] Y. S. Dedkov, M. Fonin, and C. Laubschat, Appl. Phys. Lett. **92**, 052506 (2008).
[30] C. Oshima and A. Nagashima, J. Phys.: Condens. Matter **9**, 1 (1997).
[31] Y. Gamo, A. Nagashima, M. Wakabayashi, M. Terai, and C. Oshima, Surf. Sci. **374**, 61 (1997).
[32] O. K. Andersen, O. Jepsen, and D. Glötzel, in *Highlights of Condensed Matter Theory*, Proceedings of the International School of Physics 'Enrico Fermi', Varenna, Italy, edited by F. Bassani, F. Fumi, and M. P. Tosi (North-Holland, Amsterdam, 1985), pp. 59–176.
[33] P. E. Blöchl, Phys. Rev. B **50**, 17953 (1994).
[34] G. Kresse and D. Joubert, Phys. Rev. B **59**, 1758 (1999).
[35] G. Kresse and J. Hafner, Phys. Rev. B **47**, 558 (1993).
[36] G. Kresse and J. Furthmuller, Phys. Rev. B **54**, 11169 (1996).
[37] J. Neugebauer and M. Scheffler, Phys. Rev. B **46**, 16067 (1992).
[38] P. E. Blöchl, O. Jepsen, and O. K. Andersen, Phys. Rev. B **49**, 16223 (1994).

[39] G. Giovannetti, P. A. Khomyakov, G. Brocks, V. M. Karpan, J. van den Brink, and P. J. Kelly, Phys. Rev. Lett. **101**, 026803 (2008).
[40] T. Ando, Phys. Rev. B **44**, 8017 (1991).
[41] P. A. Khomyakov, G. Brocks, V. Karpan, M. Zwierzycki, and P. J. Kelly, Phys. Rev. B **72**, 035450 (2005).
[42] K. Xia, P. J. Kelly, G. E. W. Bauer, I. Turek, J. Kudrnovský, and V. Drchal, Phys. Rev. B **63**, 064407 (2001).
[43] K. Xia, M. Zwierzycki, M. Talanana, P. J. Kelly, and G. E. W. Bauer, Phys. Rev. B **73**, 064420 (2006).
[44] M. Zwierzycki *et al.*, Phys. Status Solidi B **245**, 623 (2008).
[45] M. Büttiker, Y. Imry, R. Landauer, and S. Pinhas, Phys. Rev. B **31**, 6207 (1985).
[46] S. Datta, *Electronic Transport in Mesoscopic Systems* (Cambridge University Press, Cambridge, 1995).
[47] I. Turek, V. Drchal, J. Kudrnovský, M. Šob, and P. Weinberger, *Electronic Structure of Disordered Alloys, Surfaces and Interfaces* (Kluwer, Dordrecht, 1997).
[48] P. Soven, Phys. Rev. **156**, 809 (1967).
[49] D. Glötzel, B. Segall, and O. K. Andersen, Solid State Commun. **36**, 403 (1980).
[50] *International Tables for Crystallography*, edited by T. Hahn (Springer, New York, 2005), Vol. 1.
[51] G. Bertoni, L. Calmels, A. Altibelli, and V. Serin, Phys. Rev. B **71**, 075402 (2005).
[52] To describe the adsorption of graphite on Co and Ni within model I we use two empty spheres with a Wigner-Seitz sphere radius $r=1.12$ a.u. at *B* and *C* sites, positioned 1.57 a.u. above the metal surface. For model II we use one empty sphere with a Wigner-Seitz sphere radius $r=1.7$ a.u. at a *C* site, at 2.42 a.u. above the surface. If the distance between graphite and the metal surface is larger, which is the case for graphite on Cu, we use three empty spheres with Wigner-Seitz sphere radius $r=1.6$ a.u., at *A*, *B*, and *C* sites, respectively, 3.33 a.u. above the surface.
[53] W. H. Butler, X.-G. Zhang, T. C. Schulthess, and J. M. MacLaren, Phys. Rev. B **63**, 054416 (2001).
[54] J. Mathon and A. Umerski, Phys. Rev. B **63**, 220403(R) (2001).
[55] J.-C. Charlier, X. Gonze, and J.-P. Michenaud, Phys. Rev. B **43**, 4579 (1991).
[56] G. Giovannetti, P. A. Khomyakov, G. Brocks, P. J. Kelly, and J. van den Brink, Phys. Rev. B **76**, 073103 (2007).
[57] A. K. Geim and K. S. Novoselov, Nature Mater. **6**, 183 (2007).
[58] D. J. Monsma, R. Vlutters, and J. C. Lodder, Science **281**, 407 (1998).
[59] K. Matsubara, K. Sugihara, and T. Tsuzuku, Phys. Rev. B **41**, 969 (1990).
[60] G. Schmidt, D. Ferrand, L. W. Molenkamp, A. T. Filip, and B. J. van Wees, Phys. Rev. B **62**, R4790 (2000).